PERGAMON

International Journal of Heat and Mass Transfer 42 (1999) 4487–4500

International Journal of HEAT and MASS TRANSFER

www.elsevier.com/locate/ijhmt

Thermoconvective instability in a horizontal porous cavity saturated with cold water

M. Mamou, L. Robillard*, P. Vasseur

Ecole Polytechnique, University of Montreal, CP 6079, Succursale 'Down Town', Montreal, Quebec, Canada H3C 3A7

Received 25 November 1998; received in revised form 18 March 1999

Abstract

The onset of convection in a horizontal porous cavity with regard to the density maximum of water at 3.98°C is studied using a linear stability analysis. In the formulation of the problem use is made of the Brinkman-extended Darcy model which is relevant to sparsely packed porous media. A parabolic density-temperature relationship is used to model the effect of density inversion. The perturbation equations are solved with the aid of the Galerkin and finite element methods. The onset of motion is found to be dependent of the aspect ratio A of the cavity, the Darcy number Da, the inversion parameter γ and the hydrodynamic boundary conditions applied on the horizontal walls of the porous layer. The results for a viscous fluid ($Da \to \infty$) and the Darcy porous medium ($Da \to 0$) emerge from the present analysis as limiting cases. Numerical results for finite amplitude convection, obtained by solving the full governing equations, indicate that subcritical convection is possible when the upper stable layer extends over more than the half depth. Also, the existence of multiple solutions for a given range of governing parameters is demonstrated.

1. Introduction

Starting with the early works of Horton and Rogers [1] and Lapwood [2], the problem of the onset of convection in a horizontal fluid-saturated porous layer heated from below has been a major topic of porous media research in recent years. So far, most of the studies are concerned with fluids having a linear relationship between density and temperature. The state of the art has been summarized in a recent book by Nield and Bejan [3]. Convection in cold water, however, behaves in a complicated manner when the temperature domain encompasses the 4°C, point at which the density of water reaches a maximum value. In general, other fluids such as gallium, tellurium, antimony and molten bismuth possess a density extremum in the density–temperature relationship. However, among those fluids cold water, one of the common fluids occurring in nature, is the most important.

Relatively few studies have been concerned with the problem of the onset of convection in a horizontal porous layer saturated with cold water. Using a cubic density-temperature relationship, Sun et al. [5] were the first to establish the criterion for the onset of convection. The effects of density inversion on free convective heat transfer in a porous medium heated from below has been investigated experimentally by Yen [5]. The onset of convection was found to be dependent on two thermal parameters which are functions of the boundary temperatures and the coefficients representing the fluid density-temperature relationship. The linear stability predictions made by Sun et al. [4] were verified numerically by Blake et al. [6]. The effect of the Rayleigh

* Corresponding author. Tel.: +1-514-340-4711; fax: +1-514-340-5917.

E-mail address: robillard@meca.polymtl.ca (L. Robillard)

0017-9310/99/$ - see front matter
PII: S0017-9310(99)00103-9

Nomenclature

A	aspect ratio, W'/H'
A_C	wavelength associated to R_C
Da	Darcy number, K/H'^2
g	acceleration due to gravity
h'_m	height of the unstable layer
h'_p	height (penetration) of the convective layer
H'	overall height of the layer
k	thermal conductivity of the saturated porous medium
K	permeability of the porous medium
Nu	Nusselt number, Eq. (42)
R	Darcy–Rayleigh number, $g\beta K\Delta T'^2H'/\alpha\nu$
Ra	fluid Rayleigh number, $g\beta\Delta T'^2H'^3/\alpha\nu$
R_C	critical Darcy–Rayleigh number
R_0	ratio, R/R_C
T	dimensionless temperature, $(T'-T'_L)/\Delta T'$
T'_L	temperature of the lower boundary
T'_U	temperature of the upper boundary
T'_m	temperature of maximum density
$\Delta T'$	characteristic temperature difference, $T'_U-T'_L$
t	dimensionless time, $\sigma t'\alpha/H'^2$
W'	width of the porous layer
x, y	dimensionless coordinate system, $(x'/H', y'/H')$

Greek symbols

α	thermal diffusivity, $k/(\rho_0C)_f$
γ	inversion parameter, $2(T'_m-T'_L)/(T'_U-T'_L)$
β	coefficient, Eq. (1), $^\circ C^{-2}$
δ	coefficient, Eq. (1), $^\circ C^{-3}$
ν	kinematic viscosity of fluid
ρ	density of fluid
$(\rho_0C)_f$	heat capacity of fluid
Ψ	stream function, Ψ'/α

number, for finite amplitude convection, on the overall heat transfer rate through the layer was also documented by these authors. The onset of thermal instabilities in the vicinity of the density maximum in the presence of a time-dependent nonlinear mean temperature distribution has been investigated by Poulikakos [7]. More recently, Zhang [8] investigated numerically the problem of penetrative convection within a horizontal porous layer saturated with cold water. The critical Rayleigh and wave numbers were predicted numerically on the basis of a linear stability theory. Computations, for finite amplitude convection, indicate the existence of subcritical convection. In all the above studies the porous medium is modeled according to Darcy's law. This is found to give satisfactory results when the porous medium is closely packed and with low porosity.

The objective of the present study, based on the linear stability analysis, is to extend the results in Refs. [4] and [7] for the case of sparsely packed porous media. In the formulation of the model, use is made of the Brinkman-extended Darcy formulation [9]. A parabolic density-temperature relationship is used to model the effect of density inversion. The predicted critical Rayleigh numbers bridge the gap between viscous fluid and low permeability porous medium.

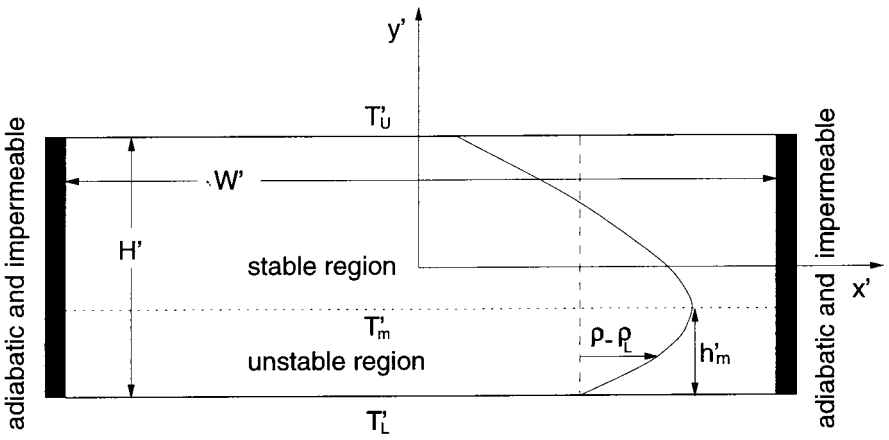

Fig. 1. Geometry of the physical problem.

2. Problem description and mathematical model

The physical system of interest is the two-dimensional enclosure shown in Fig. 1. The system is filled with a water saturated porous medium. The Brinkman-extended Darcy model, which is relevant to sparsely packed porous media, is used in the present study. The flow in the enclosure is assumed laminar and the dissipation effects are neglected. Also, the water is modeled as a Boussinesq-incompressible fluid whose physical properties are constant except the density, in the buoyancy force, which may be considered to vary with the temperature according to the cubic relationship [4]

$$\rho = \rho_m[1 - \beta(T' - T'_m)^2 - \delta(T' - T'_m)^3] \tag{1}$$

with T'_m being the temperature at which the maximum density ρ_m is obtained.

In above equation, the values $T'_m = 3.98°C$, $\beta = 7.94 \times 10^{-6}\ °C^{-2}$ and $\delta = -6.56 \times 10^{-8}\ °C^{-3}$ stand for pure water. The resulting relation was found to be valid in the range 0–30°C [10].

The flow and the heat transfer inside the enclosure are governed by the continuity, momentum and energy conservation equations. They are stated by

$$\nabla \vec{V}' = 0 \tag{2}$$

$$\vec{V}' = \frac{K}{\mu}[-\nabla P' + \mu_{eff}\nabla^2 \vec{V}' + \rho \vec{\mathbf{g}}] \tag{3}$$

$$\sigma \frac{\partial T'}{\partial t'} + \vec{V}' \cdot \nabla T' = \frac{k}{(\rho_0 C)_f} \nabla^2 T' \tag{4}$$

where K is the permeability of the porous matrix, $\vec{V}'$ is the mass-averaged velocity, $\vec{\mathbf{g}}$ is the gravity vector and $(\rho_0 C)_f$ is the heat capacity of fluid with reference density ρ_0.

In the present problem, the unknown variables are the velocity components (u', v'), pressure P' and temperature T'. It is convenient to introduce the stream function Ψ' defined by

$$u' = \frac{\partial \Psi'}{\partial y'}, \quad v' = -\frac{\partial \Psi'}{\partial x'} \tag{5}$$

such that the continuity Eq. (2) is automatically satisfied.

Upon introducing the above equation and taking the curl of the momentum equation, one obtains

$$\nabla^2 \Psi = r_\mu Da \nabla^4 \Psi - R \mathscr{F}(T) \frac{\partial T}{\partial x} \tag{6}$$

In the above equation, the viscosity ratio $r_\mu = \mu_{eff}/\mu$ is in general made equal to unity (see, for instance, Nield and Bejan [3]).

The dimensionless energy equation takes the following form

$$\frac{\partial T}{\partial t} - \mathscr{J}(\Psi, T) = \nabla^2 T \tag{7}$$

The operators $\mathscr{F}$ and $\mathscr{J}$ are expressed as follows

$$\mathscr{F}(T) = \left[-\gamma\left(1 + \frac{3}{4}\theta\gamma\right) + 2\left(1 + \frac{3}{2}\theta\gamma\right)T - 3\theta T^2 \right]$$

$$\mathscr{J}(\Psi, T) = \frac{\partial \Psi}{\partial x}\frac{\partial T}{\partial y} - \frac{\partial \Psi}{\partial y}\frac{\partial T}{\partial x} \tag{8}$$

where γ and θ are defined as

$$\gamma = 2\frac{T'_m - T'_L}{\Delta T'}, \quad \theta = \frac{\delta}{\beta}\Delta T', \quad \Delta T' = T'_U - T'_L \tag{9}$$

The above dimensionless governing equations have been obtained by introducing the following dimensionless variables:

$$(x, y) = \left(\frac{x'}{H'}, \frac{y'}{H'}\right), \quad \vec{V} = \frac{\vec{V}' H'}{\alpha}, \quad t = \frac{t'\sigma\alpha}{H'^2}, \quad T = \frac{(T' - T'_L)}{\Delta T'} \tag{10}$$

The governing Eqs. (6) and (7) contain five dimensionless governing parameters, namely the Darcy–Rayleigh number, R, the Darcy number, Da, the aspect ratio of the enclosure, A, and the parameters, γ and θ. The parameters R, Da and A are defined as

$$R = \frac{gK\beta\Delta T' 2H'}{\alpha\nu}, \quad Da = \frac{K}{H'^2}, \quad A = \frac{W'}{H'} \tag{11}$$

In the past, Moore and Weiss [10] and Musman [11] have used a dimensionless Rayleigh number based on the depth of the unstable layer h'_m and on the difference in density across the unstable layer. Thus, with the following relationships

$$0<\gamma<2: \quad h'_m = H'\left(\frac{\gamma}{2}\right), \quad \Delta T'_m = \Delta T'\left(\frac{\gamma}{2}\right)$$

$$\gamma \geq 2: \quad h'_m = H', \quad \Delta T'_m = \Delta T' \tag{12}$$

we define the modified Rayleigh and Darcy numbers and the modified aspect ratio as

$$0<\gamma<2: \quad R_m = R\left(\frac{\gamma}{2}\right)^3, \quad Da_m = Da\left(\frac{2}{\gamma}\right)^2, \quad A_m = A\left(\frac{2}{\gamma}\right)$$

$$\gamma \geq 2: \quad R_m = R(\gamma - 1), \quad Da_m = Da, \quad A_m = A \tag{13}$$

The hydrodynamic boundary conditions on all the solid boundaries are expressed by

$$\Psi = \frac{\partial \Psi}{\partial n} = 0 \tag{14}$$

where n is the normal direction with respect to the boundaries. For a free boundary, the hydrodynamic boundary conditions are

$$\Psi = \frac{\partial^2 \Psi}{\partial n^2} = 0 \tag{15}$$

In this study the hydrodynamic boundary condition applied on the lower and the upper horizontal walls of the cavity are rigid-rigid, free-free and rigid-free. In the following text, the abbreviations RR, FF and RF will be used to represent these three types of boundary conditions.

The thermal boundary conditions are given by

$$x = \pm\frac{A}{2}: \quad \frac{\partial T}{\partial x} = 0 \quad \text{and} \quad y = \pm\frac{1}{2}: \quad T = 1, 0 \tag{16}$$

For the infinite slender enclosure ($A \to \infty$), in which the flow structure reveals periodical counterrotating cells, periodic boundary conditions in x-direction ($\varphi(x, y) = \varphi(x + A_C, y)$, where φ stands for Ψ and T and A_C is the wavelength) are considered.

The Brinkman model described above represents an intermediate case between the clear fluid and the Darcy model (see, for instance, Vasseur and Robillard, [12]). The transition from one to the other is obtained by decreasing Da from infinity to zero. In practice, the value $Da = 10$ is considered in the present work to represent very closely the fluid behavior. Conversely, the Darcy behavior is assumed to be practically reached at $Da = 10^{-6}$.

3. Linear stability analysis

In this section a marginal linear stability analysis is used to predict the critical Rayleigh number for the onset of convection. As usual, we introduce the following transformation

$$\Psi(x, y) = \Psi_R + \psi(x, y)$$

$$T(x, y) = T_R + \phi(x, y) \tag{17}$$

where $\Psi_R = 0$ and $T_R = y + 1/2$ correspond to the rest state and $\psi(x, y)$ and $\phi(x, y)$ are the perturbed solution resulting from the convective effects.

Assuming separability, the steady perturbed solution can be written as follows

$$\psi(x, y) = \psi_0 F(x, y) \quad \text{and} \quad \phi(x, y) = \phi_0 G(x, y) \tag{18}$$

where the amplitudes ψ_0 and ϕ_0 are small constants.

Substituting the rest-state solution and the small perturbations, Eqs. (17) and (18), into the governing Eqs. (6) and (7) and discarding the second order terms involving the perturbations (at the beginning of convection, the amplitudes ψ_0 and ϕ_0 are close to zero), the following linearized set of governing equations is obtained

$$\psi_0 \nabla^2 F = Da\psi_0 \nabla^4 F - Rf(y)\phi_0 \frac{\partial G}{\partial x} \tag{19}$$

$$-\psi_0 \frac{\partial F}{\partial x} = \phi_0 \nabla^2 G \tag{20}$$

where $f(y)$ is a quadratic function of y:

$$f(y) = \frac{1-\gamma}{4}[4 - 3\theta(1-\gamma)] + [2 - 3\theta(1-\gamma)]y - 3\theta y^2 \tag{21}$$

The boundary conditions for the function $F(x, y)$ are similar to those of $\Psi(x, y)$ depicted in Eqs. (14) and (15). However, the boundary condition for $G(x, y)$ are

$$x = \pm\frac{A}{2}: \quad \frac{\partial G}{\partial x} = 0 \quad \text{and} \quad y = \pm\frac{1}{2}: \quad G = 0 \tag{22}$$

The above linear governing equations can be solved numerically using the finite element method. To this end, we introduce the Galerkin method to turn the linear equations into the weak formulation. Multiplying Eq. (19) by $w(x, y)$ and Eq. (20) by $\vartheta(x, y)$, integrating using the Green's theorem, we obtain

$$\psi_0 \int_\Omega \nabla F \nabla w \, d\Omega + \psi_0 Da \int_\Omega \nabla^2 F \nabla^2 w \, d\Omega = \phi_0 R \int_\Omega f(y) \frac{\partial G}{\partial x} w \, d\Omega \quad \forall w \in H^2(\Omega) \tag{23}$$

$$-\psi_0 \int_\Omega \frac{\partial F}{\partial x}\vartheta \, d\Omega = -\phi_0 \int_\Omega \nabla G \nabla \vartheta \, d\Omega + \phi_0 \int_\Gamma \frac{\partial G}{\partial n} \vartheta \, d\Gamma \quad \forall \vartheta \in H^2(\Omega) \tag{24}$$

where $w(x, y)$ and $\vartheta(x, y)$ are arbitrary test functions and $H^2(\Omega)$ is the Hilbert space having square inte-

grable functions including their first and second derivatives.

The finite element method is employed to solve the above set of equations. The solution domain is first discretized into finite elements Ω^e such that $\Omega = \cup_{i=1}^{n_e} \Omega^e$, where n_e is the number of elements. With the stream function formulation, the maximum order of the linear partial differential equations is four. For this reason a rectangular Hermite cubic element of high precision has been chosen. The degrees of freedom at each node involve the value of the function, its two first derivatives and its cross derivative.

3.1. Confined enclosure

Within each element, the functions $F(x, y)$ and $G(x, y)$ are expressed in the general form

$$\begin{Bmatrix} F(x,y) \\ G(x,y) \end{Bmatrix} = \sum_{j=1}^{4} \begin{bmatrix} F_j & \frac{\partial F_j}{\partial x} & \frac{\partial F_j}{\partial y} & \frac{\partial^2 F_j}{\partial x \partial y} \\ G_j & \frac{\partial G_j}{\partial x} & \frac{\partial G_j}{\partial y} & \frac{\partial^2 G_j}{\partial x \partial y} \end{bmatrix}^e \begin{Bmatrix} \mathcal{N}_j(x,y) \\ \mathcal{N}_{j+4}(x,y) \\ \mathcal{N}_{j+8}(x,y) \\ \mathcal{N}_{j+12}(x,y) \end{Bmatrix} \quad (25)$$

where $\mathcal{N}_j(x, y)$ are the Hermite interpolation functions.

Using the approximation (25) and choosing the interpolation functions $\mathcal{N}_i(x, y)$ as the weighted functions, after assembling in terms of global matrices and solutions vectors $\{F\}$ and $\{G\}$, Eqs. (23) and (24) reduce to the following discretized set of linear equations

$$\psi_0[K_\psi]\{F\} = R\phi_0[B]\{G\} \quad (26)$$

$$\psi_0[L]\{F\} = \phi_0[K]\{G\} \quad (27)$$

where $[B]$, $[K_\psi]$, $[K]$ and $[L]$ are $m \times m$ square matrices, where $m = 4N_n$ and N_n is the total nodes number defined as $N_n = (N_{ex}+1)(N_{ey+1})$ in which N_{ex} and N_{ey} are the number of elements in x- and y-directions, respectively. The corresponding elementary matrices can be computed from the following integrals

$$[B]^e = \int_{\Omega^e} f(y) \frac{\partial \mathcal{N}_j}{\partial x} \mathcal{N}_i \, d\Omega,$$

$$[K]^e = \int_{\Omega^e} \nabla \mathcal{N}_j \cdot \nabla \mathcal{N}_i \, d\Omega$$

$$[L]^e = \int_{\Omega^e} \frac{\partial \mathcal{N}_j}{\partial x} \mathcal{N}_i \, d\Omega,$$

$$[K_\psi]^e = \int_{\Omega^e} (\nabla \mathcal{N}_j \cdot \nabla \mathcal{N}_i + Da \, \nabla^2 \mathcal{N}_j \cdot \nabla^2 \mathcal{N}_i) d\Omega \quad (28)$$

and $\{F\}$ and $\{G\}$ are solution vectors of length m.

It is noted that the boundary integrals, known as the natural boundary conditions, vanish for the homogenous Dirichlet and Neumann boundary conditions.

Substituting Eq. (27) into (26), we obtain the following eigenvalue problem equation

$$\psi_0[[E] - \lambda[I]]\{F\} = 0$$

$$[E] = [K_\psi]^{-1}[B][K]^{-1}[L] \quad (29)$$

where $[I]$ is the identity matrix, $\lambda = 1/R$ represents the eigenvalue and $\{F\}$ the eigenvector.

From a mathematical point of view, Eq. (29) has a non-trivial solution ($\{F\} = 0$) if and only if the determinant of $[E-\lambda I]$ is equal to zero. This leads to the computation of all the eigenvalues, $\lambda_i (i = 1, m)$ of the matrix $[E]$ by using for instance, the subroutine (DE2CRG) of the IMSL library. In general, λ_i are complex numbers. For the present case, they are real and can be rearranged as $\lambda_1 \le \lambda_2 \le \ldots \le \lambda_{m-1} \le \lambda_m$. According to the inversion parameters values γ and θ, the values of λ_i can be positive or negative. From Eq. (29), it is seen that positive values correspond to $R > 0$ and negative values to $R < 0$ (reverse gravity)), those negative values being irrelevant. Thus, the critical Rayleigh number for the onset of convection is given by

$$R_C = \frac{1}{\lambda_m}. \quad (30)$$

The precision of the present numerical procedure depends, naturally, on the grid numbers. The fluid that saturates the porous matrix is a standard Boussinesq incompressible fluid whose density variation can be expressed as a linear equation of state. With the present mathematical model, this behavior can be obtained for $\gamma \to \infty$ (in practice, $\gamma \sim 10^4$). Darcy number values of 10^{-6} and 10^3 are chosen to model the pure Darcy porous medium and the fluid medium (RR boundaries), respectively. For the Darcy medium the linear Rayleigh number $R_{mC} = 4\pi^2 = 39.478$ has been predicted analytically in the past by Horton and Rogers [1] and Lapwood [2], on the basis of the linear stability theory. The value $Ra_{mC} = 2585.03$ has been obtained numerically by Platten and Legros [13] for the fluid medium with rigid-rigid boundaries. In the present work, using different grid sizes ($N_{ex} \times N_{ey}$) 4×4, 8×8 and 16×16 the values of the critical

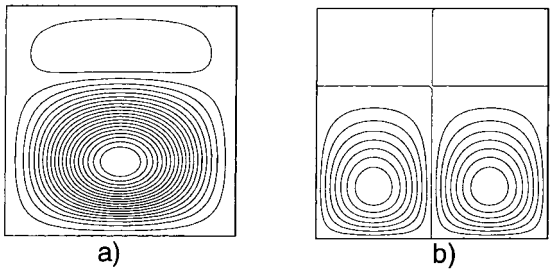

Fig. 2. Incipient flow patterns for a square enclosure with $\gamma = 1$: (a) clear fluid with RR boundaries ($Ra_{mC} = 787.4$); (b) pure Darcy medium ($R_{mC} = 31.4$).

Rayleigh number for the case of clear fluid are 2596.72, 2585.92 and 2585.13, respectively, and those of the pure Darcy case are 39.480, 39.479 and 39.479. Based on the results, it is clear that a grid size of 8×8 or more is sufficient to model accurately the problem. In the present study, depending on the value of γ, a grid size of 10×10 to 20×20 is considered for a square enclosure.

The differences between a parabolic and a cubic relation for predicting the density-temperature behavior of water, around the maximum density region, will be now discussed. The effect of the inversion parameter θ (see Eq. (9)) on the critical Rayleigh number has been studied for a square cavity with RR boundaries, for $\gamma = 1$ and $Da_m = 4 \times 10^{-2}$. The case $\gamma = 1$ for which the maximum density is located at mid height of the enclosure, corresponds to the existence of a stable layer in the upper half of the cavity and an unstable layer in the lower one. The cases $\theta = 0$ and θ different from zero correspond to parabolic and cubic density-temperature relationships, respectively. The results indicate that upon increasing θ from 0 to 10^{-1}, the critical Rayleigh number increases from 72.804 to 76.216 which corresponds to a maximum variation of 4.7%. The difference between values of the critical Rayleigh number, calculated from parabolic or cubic relationships, for the temperature range of interest in this study (0–8°C) is found to be very small. For this reason, a parabolic equation of state ($\theta = 0$) will be used in this study for its simplicity.

Using the parabolic state equation for clear fluid with RR boundaries and pure Darcy medium for the case of a square cavity with $\gamma = 1$ gives $Ra_{mC} = 787.4$ and $R_{mC} = 31.49$. The corresponding flow patterns at the onset of convection are presented in Fig. 2. They differ by the number of convective cells (one for the fluid case and two for the Darcy one). Both are characterized by a weak circulation at the top of the cavity. It is clear from Fig. 2 that the induced convective cell is not limited to the thickness of the unstable layer but penetrates considerably inside the stable layer

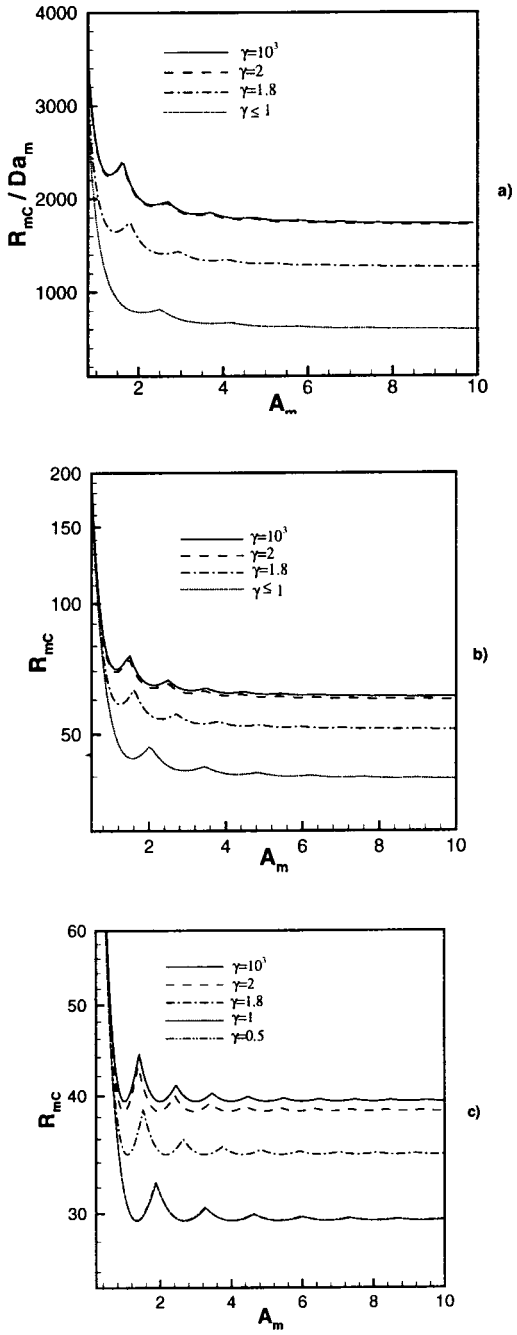

Fig. 3. Effect of the aspect ratio A_m and inversion parameter γ on the critical Rayleigh number, R_{mC}: (a) clear fluid with RR boundaries; (b) Brinkman medium with $Da_m = 10^{-2}$ and RR boundaries; (c) pure Darcy medium.

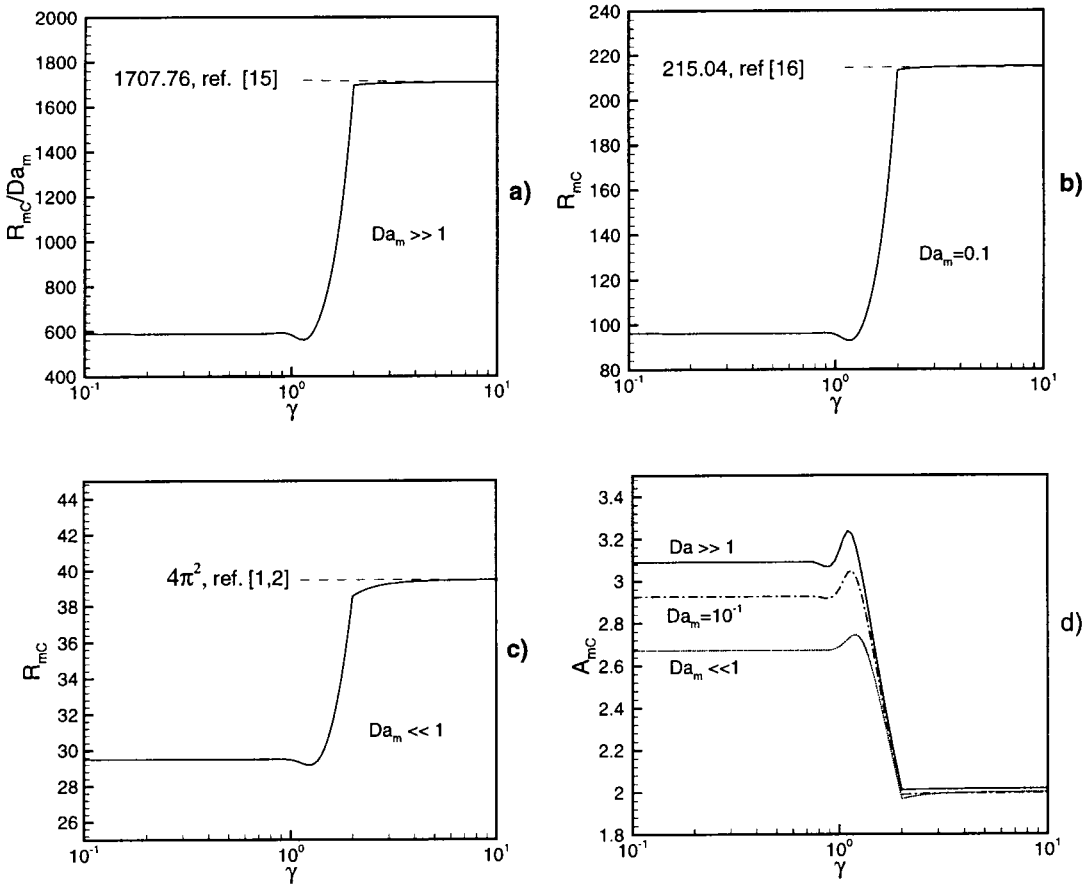

Fig. 4. Effect of the inversion parameter γ on the critical Rayleigh number R_{mC} in a layer of infinite lateral extent: (a) clear fluid with RR boundaries; (b) Brinkman medium with $Da_m = 10^{-1}$ and RR boundaries; (c) pure Darcy medium; (d) corresponding critical wavelength A_{mC}.

with the maximum penetration for the fluid case. Thus with R_m increased beyond the threshold, the initial motion induces a mixing between fluid layers on each side of the maximum density with the result that the unstable layer is enlarged.

The effect of the aspect ratio, A_m, on the critical Rayleigh number is shown in Fig. 3(a)–(c) for the clear fluid, an intermediate case ($Da_m = 10^{-2}$) and the pure Darcy medium. It can be seen on each graph that R_{mC} undergoes an irregular variation passing through maximums and minimums, when increasing the aspect ratio A_m. Each peak indicates that the number of convective cells is increased by one. As the aspect ratio increases towards large values, R_{mC} tends asymptotically towards the constant value corresponding to a layer of infinite extent. Furthermore, it is observed that results for the fluid medium, Fig. 3(a), fall on a single curve for $\gamma > 2$. This is not quite the same for the Darcy medium, Fig. 3(c), where nearly spaced but distinct curves are shown for $\gamma = 2$ and $\gamma = 10^3$. Nevertheless, the upper curve in each of the three graphs represents an asymptotic behavior for large γ. The same is true for the lower curve which represents all the cases within the range $0 < \gamma < 1$. The fact that the upper and lower curves in each of these graphs are asymptotic limits for $\gamma > 2$ and $\gamma < 1$, respectively, results from the present normalization of A and Da

3.2. Infinite horizontal enclosure

For this situation the perturbed solution can be written as follows

$$\psi(x, y) = \psi_0 \sin \omega\, x F(y)$$

$$\phi(x, y) = \phi_0 \cos \omega x\, G(y) \tag{31}$$

where ω is the wavenumber defined as $\omega = 2\pi/A_C$ and A_C is the critical wavelength.

Substituting (17) and (31) into the governing Eqs.

(6) and (7) and discarding the second order terms, the linearized governing equations are obtained as follows

$$\psi_0\left(\frac{d^2F}{dy^2}-\omega^2F\right) = Da\,\psi_0\left(\frac{d^4F}{dy^4}-2\omega^2\frac{d^2F}{dy^2}+\omega^4F\right)-\omega\,Rf(y)\phi_0G \quad (32)$$

$$\omega\psi_0F=-\phi_0\left(\frac{d^2G}{dy^2}-\omega^2G\right) \quad (33)$$

where $f(y)$ is defined by (21).

Following the numerical procedure described above for the case of a confined enclosure, the discretization of Eqs. (32) and (33) yields matrix systems similar to those given by Eqs. (26) and (27). For the present case, the elementary matrices are defined now as

$$[B]^e=\int_{\Delta y^e}\omega f(y)\mathcal{N}_j\mathcal{N}_i\,dy,$$

$$[K]^e=\int_{\Delta y^e}\left(\frac{d\mathcal{N}_j}{dy}\frac{d\mathcal{N}_i}{dy}+\omega^2\mathcal{N}_j\mathcal{N}_i\right)dy,$$

$$[L]^e=\int_{\Delta y^e}\omega\mathcal{N}_j\mathcal{N}_i\,dy$$

$$[K_\psi]^e=\int_{\Delta y^e}\left(Da\frac{d^2\mathcal{N}_j}{dy^2}\frac{d^2\mathcal{N}_i}{dy^2}+(1+2Da\omega^2)\frac{d\mathcal{N}_j}{dy}\frac{d\mathcal{N}_i}{dy}+\omega^2(1+Da\omega^2)\mathcal{N}_j\mathcal{N}_i\right)dy \quad (34)$$

$\{F\}$ and $\{G\}$ are solution vectors of length $m_y=4(N_{ey}+1)$ and Δy^e is the finite element length.

The above matrix system can be combined to yield an eigenvalue problem similar to that given by Eq. (29). For a given set of the governing parameters Da and γ, the critical Rayleigh number R_C is computed for different values of the enclosure aspect ratio A. The minimum value of R_C and the corresponding aspect ratio A_C give the critical Rayleigh number for the onset of convection and the critical wavenumber of the convective rolls, respectively.

To validate our numerical code, we have considered the classical Bénard problem for an infinite horizontal porous layer. The case of a pure Darcy medium ($Da\to 0$) was considered first. Using the values $Da_m=10^{-6}$ and $\gamma=10^4$, the computed critical Darcy Rayleigh number, R_{mC}, and the corresponding wavelength ($\omega=2\pi/A_{mC}$) with 40 elements in y-direction are given by 39.483 and 3.142, respectively, in agreement with the values $R_{mC}=4\pi^2$ and $\omega=\pi$ predicted analytically (Refs. [1,2]), on the basis of the linear stability analysis. Similarly, using the values $Da=10^3$ and $\gamma=10^4$ the critical Rayleigh number and the corresponding wavenumber for a pure fluid were obtained as $Ra_{mC}=1707.807$ and $\omega=2\pi/A_{mC}=3.116$ in agreement with the results obtained by Chandrasekhar [14].

Fig. 4 shows the critical Rayleigh number R_{mC} and the corresponding wavelength A_{mC} for an infinite layer, with RR boundaries, as functions of the inversion parameter γ. Three cases, namely the fluid

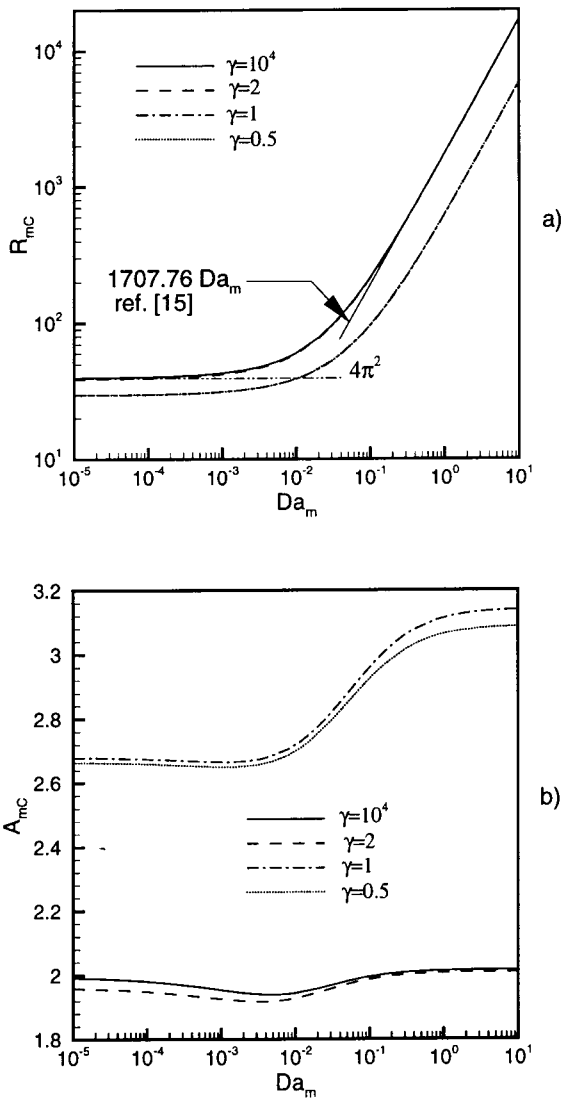

Fig. 5. Effect of the Darcy number Da_m and of the inversion parameter γ in a layer of infinite lateral extent with RR boundaries: (a) critical Rayleigh number R_{mC}; (b) corresponding wavelength A_{mC}.

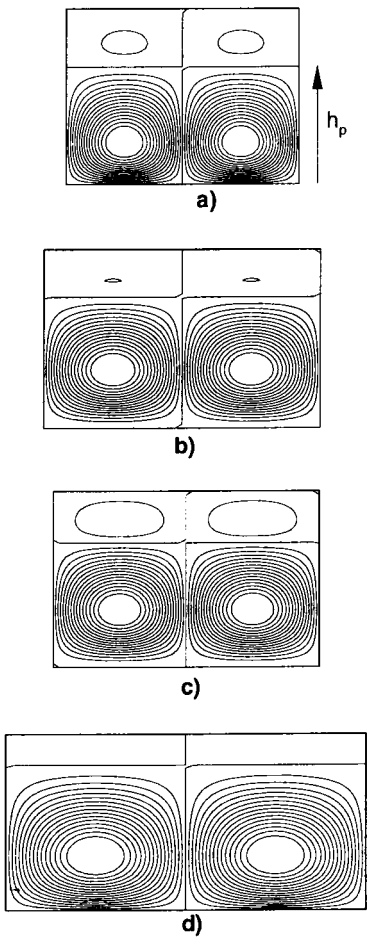

Fig. 6. Effect of the Darcy number Da_m on the incipient flow field in a layer of infinite lateral extent with $\gamma = 1$: (a) pure Darcy medium ($R_{mC} = 29.46$; $A_{mC} = 2.688$); (b) clear fluid with RR boundaries, ($R_{mC} = 583.31$; $A_{mC} = 3.140$); (c) clear fluid with RF boundaries ($R_{mC} = 593.06$; $A_{mC} = 3.074$), (d) clear fluid with FF boundaries ($R_{mC} = 265.60$; $A_{mC} = 4.149$).

medium, Fig. 4(a), an intermediate case ($Da_m = 10^{-1}$), Fig. 4(b), with RR boundaries and the pure Darcy medium, Fig. 4(c), are considered. The limiting values $\gamma \to \infty$ and $\gamma \to 0$ correspond, respectively, to the linear relationship ρ vs T and to a stable layer of a very large thickness. Thus for $\gamma \to \infty$, we obtain the limiting values reported by Refs. [1,2,14] for the pure Darcy and the fluid medium, respectively. For the other limit $\gamma \to 0$, we obtain $Ra_{mC} = 589.310$ for the fluid medium and $R_{mC} = 29.501$ for the Darcy medium. Fig. 4(d) shows the corresponding wavelengths. Upon decreasing γ from ∞ to 2, R_{mC} remains almost unchanged for the curves of Fig. 4(a) and (b). However there is a noticeable decrease for the Darcy medium, Fig. 4(c) and this behavior explains why the $\gamma = 2$ curve on Fig. 3(c) does not reach the asymptotic curve for large γ. For the range $\gamma \geq 2$, the unstable layer occupies the whole depth and the nonlinearity ρ vs T has little effect on the system. At $\gamma = 2$, however, all curves show a drastic change with R_{mC} starting to decrease rather abruptly. That change is related to the appearance of a stable layer near the top boundary. With γ decreasing further, a minimum is reached, followed by a slight increase to a final level. The curves of Fig. 4(d) giving the critical wavelength follow a reverse trend. The above results are similar to those reported by Musman [11] for the case of FF boundaries.

Fig. 5(a) and (b) shows the critical Rayleigh number, R_{mC} and associated critical wavelength, A_{mC}, respectively, as functions of the Darcy number, Da_m, for a layer with RR boundaries. It can be noticed on Fig. 5(a) that R_{mC} increases at first slowly with Da increasing from 10^{-5} to 10^{-2}; the change in R_{mC} becomes more important with Da_m increased further. The asymptotic values of a porous medium are obtained with $Da \to 0$ and those of a fluid with $Ra_{mC} = R_{mC}/Da_m$ are reached when $Da_m \to \infty$. Fig. 5(b) shows the variation of A_{mC} with Da_m. For $\gamma \leq 1$, A_{mC} is observed to increase with Da_m. However, for $\gamma \geq 2$, the wavelength decreases slightly, passing through a minimum at $Da_m \simeq 5 \times 10^{-3}$, then increases towards asymptotic value.

Four sets of incipient flow fields for a layer of infinite extent, are shown in Fig. 6. One corresponds to the Darcy limit ($Da_m \ll 1$) and the three others, to fluid limit ($Da_m \gg 1$) with RR, RF and FF boundaries. All those incipient fields are eigenvectors $\{\psi\}$ associated to the critical Rayleigh numbers, as obtained for $\gamma = 1$, value at which the maximum density in pure conduction is at mid-height of the enclosure. One can note that every flow field represented in that figure penetrates into the stable layer ($h_p > h_m = 0.5$, with h_p defined in Fig. 6(a) with the greatest penetration for the fluid layer. Among the three different flow fields corresponding to the fluid limit, the one with FF boundaries has the maximum penetration. Changing the upper boundary condition from rigid (RR) to free (RF) has little effect on the threshold for this value of γ, the velocity being very weak near that boundary. In each flow pattern, the weak circulation observed in the stable region is induced by the main flow cells generated in the unstable region. As mentioned earlier, the incipient penetration (penetration at incipient convection) is responsible for the existence of subcritical motion and the range of subcritical motion should be particularly important for the fluid medium with FF boundaries since it has the maximum penetration.

4. Finite amplitude convection

4.1. Numerical approach

The full set of governing Eqs. (6) and (7) has been solved numerically, for the pure Darcy limit ($Da_m \to 0$), using a finite element method based on the nine-noded Lagrangian cubic element. In the energy equation, the term involving temporal derivative is discretized using second-order backward finite difference schemes. For spatial discretization, the physical domain is divided into rectangular elements known as the nine-noded Lagrangian cubic elements, with non-uniform grid. In each element, the unknown profiles of $\Psi(x, y)$ and $T(x, y)$ are expressed as

$$\begin{Bmatrix} \Psi(x,y) \\ T(x,y) \end{Bmatrix} = \sum_{j=1}^{9} \mathcal{N}_j(x,y) \begin{Bmatrix} \Psi_j^e \\ T_j^e \end{Bmatrix} \tag{35}$$

where $\mathcal{N}_j(x, y)$ are the Lagrangian shape functions and Ψ_j^e and T_j^e are the elementary nodal values.

Using the Bubnov–Galerkin procedure with the fully implicit scheme, the discretized governing equations, after being assembled into global systems, are given in terms of the following matrical systems

$$[K_\Psi]\{\Psi_k^n\} = R_T[B]\{T_{k-1}^n\} \tag{36}$$

$$\left[\frac{1}{\Delta t^o}[M] - [C] + [K]\right]\{T_k^n\} = \frac{1}{\Delta t^o}[M]\{T^o\} \tag{37}$$

where $[B]$, $[C]$, $[K_\Psi]$, $[K]$ and $[M]$ are $m \times m$ global matrices and m is the total node number in the calculus domain ($m = (2N_{ex}+1)(2N_{ey}+1)$ where N_{ex} and N_{ey} are the numbers of elements in x and y-direction); $T^o = 4T^{k-1}/3 - T^{k-2}/3$ and $\Delta t^o = 2\Delta t/3$ (k, $k-1$ and $k-2$ correspond to t, $t-\Delta t$ and $t-2\Delta t$, respectively, and Δt being the time step).

The elementary matrices are defined by

$$[B]^e = \int_{\Omega^e} \mathcal{F}(T_k^n) \frac{\partial \mathcal{N}_j}{\partial x} \mathcal{N}_i \, d\Omega,$$

$$[C]^e = \int_{\Omega^e} J(\Psi_k^n, \mathcal{N}_j) \mathcal{N}_i \, d\Omega$$

$$[K_\Psi]^e = \int_{\Omega^e} \nabla \mathcal{N}_j \cdot \nabla \mathcal{N}_i \, d\Omega$$

$$[K]^e = \int_{\Omega^e} \nabla \mathcal{N}_j \nabla \mathcal{N}_i \, d\Omega$$

$$[M]^e = \int_{\Omega^e} \mathcal{N}_j \mathcal{N}_i \, d\Omega \tag{38}$$

To perform exactly the above integrals, four Gauss integration points are used for the matrix $[B]^e$ and three for the others.

At a given time step n and iteration k, the Darcy and the energy Eqs. (36) and (37) are solved by evaluating the temperature in the buoyancy term of Eq. (36) and the stream function in the advective terms of Eq. (37) with the previous results obtained at iteration $k-1$. The convergence of the iterative procedure is obtained when

$$\frac{\Sigma_i \, | f_i^k - f_i^{k-1} |}{\Sigma_i \, | f_i^k |} \leq 10^{-6} \tag{39}$$

where f stands for Ψ and T. In general, one to three iterations were sufficient to achieve the convergence criteria.

The linear system (36) is solved by the successive over-relaxation method. On the other hand, the linear system given by (37) is solved by an iterative procedure using the pentadiagonal matrix algorithm (PDMA) by transforming Eq. (37) as follows

$$[PD]\{T^k\} = [PD]\{T^{k-1}\} + \zeta(\{b\} - [E]\{T^{k-1}\}) \tag{40}$$

where $[PD]$ is the pentadiagonal matrix of $[E]$, ζ is the under-relaxation coefficient ($0 < \zeta < 1$) and k denotes iteration k. Here $[E]$ and $\{b\}$ are given by

$$[E] = \left[\frac{1}{\Delta t^o}[M] - [C] + [K]\right], \qquad \{b\} = \frac{1}{\Delta t^o}[M]\{T^o\} \tag{41}$$

At each time step, the convergence criterion given by Eq. (39) is used.

With the approach described above, a grid size from 20×20 to 50×20 elements was used, depending on the parameter values R and γ. For $\gamma \leq 1$, a non uniform grid size was used in the vertical direction with 15 elements in the unstable region and 5 in the stable one.

5. Results and discussion

All results shown in this part are limited to $1/3 < \gamma < 2$ and to a square cavity ($A = 1$). According to Moore and Weiss [10], stable subcritical convection of finite amplitude will exist for the fluid limit provided that $\gamma \leq 1.04$. At $\gamma = 1.04$, the upper stable region occupies nearly half of the total depth. Computations done with the present code indicate that this is also roughly the case for a Darcy medium contained in a

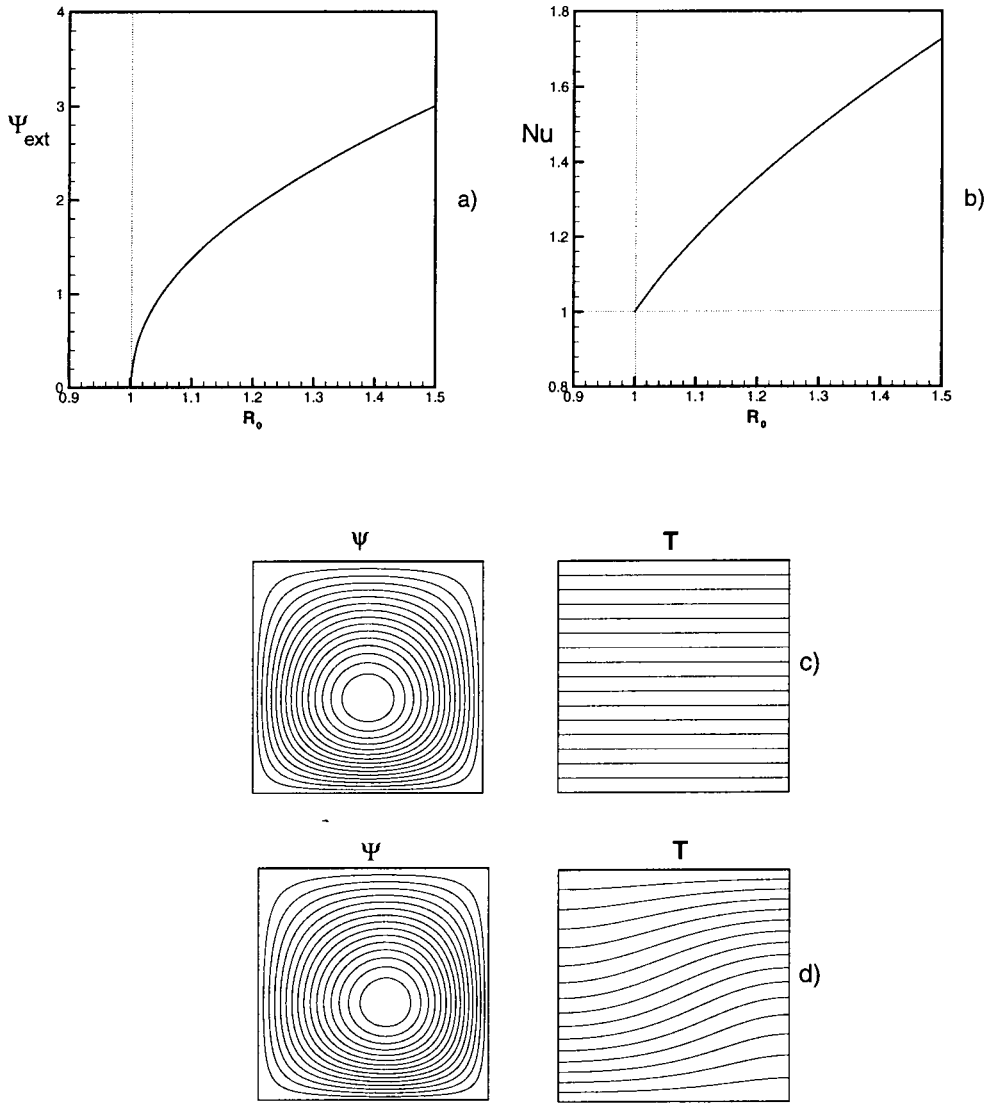

Fig. 7. Finite amplitude convection at $\gamma = 2$ for a pure Darcy medium: (a) Ψ_{ext} function of R_0; (b) Nu function of R_0; (c) incipient flow pattern and isotherms ($R_{mC} = 38.55$); (d) flow pattern and isotherms at $R_0 = 1.04$.

square cavity. Figs. 7–9 show the extremum values of the stream function (Ψ_{ext}) and the Nusselt number given as functions of the ratio $R_0 = R_m/R_{mC}$ for three different value of $\gamma(\gamma = 2, 1$ and $1/3)$. The Nusselt number is defined as

$$Nu = \int_{-1/2}^{1/2} \left.\frac{\partial T}{\partial y}\right|_{y=\pm 1/2} \mathrm{d}x \tag{42}$$

Some flow and temperature fields corresponding to those specific values of γ values are shown in the figures. For comparison, incipient flow fields (eigenvectors $\{\psi\}$ as established by the linear stability approach) are also given.

Fig. 7(a) and (b) illustrates a standard supercritical bifurcation as it exists for the classical Bénard problem. Any perturbation brought to the system at $R_0 < 1$ is resorbed. The flow field, Fig. 7(d), corresponds to a Rayleigh number just above the critical Rayleigh number $R_0 = 1.037$ and is very similar to the incipient flow field, Fig. 7(c). With $R_0 \to 1$, the flow field of Fig. 7(d) would evolve smoothly towards the one of Fig. 7(c). One particular aspect of Fig. 7(d) is the absence of symmetry with respect to the center.

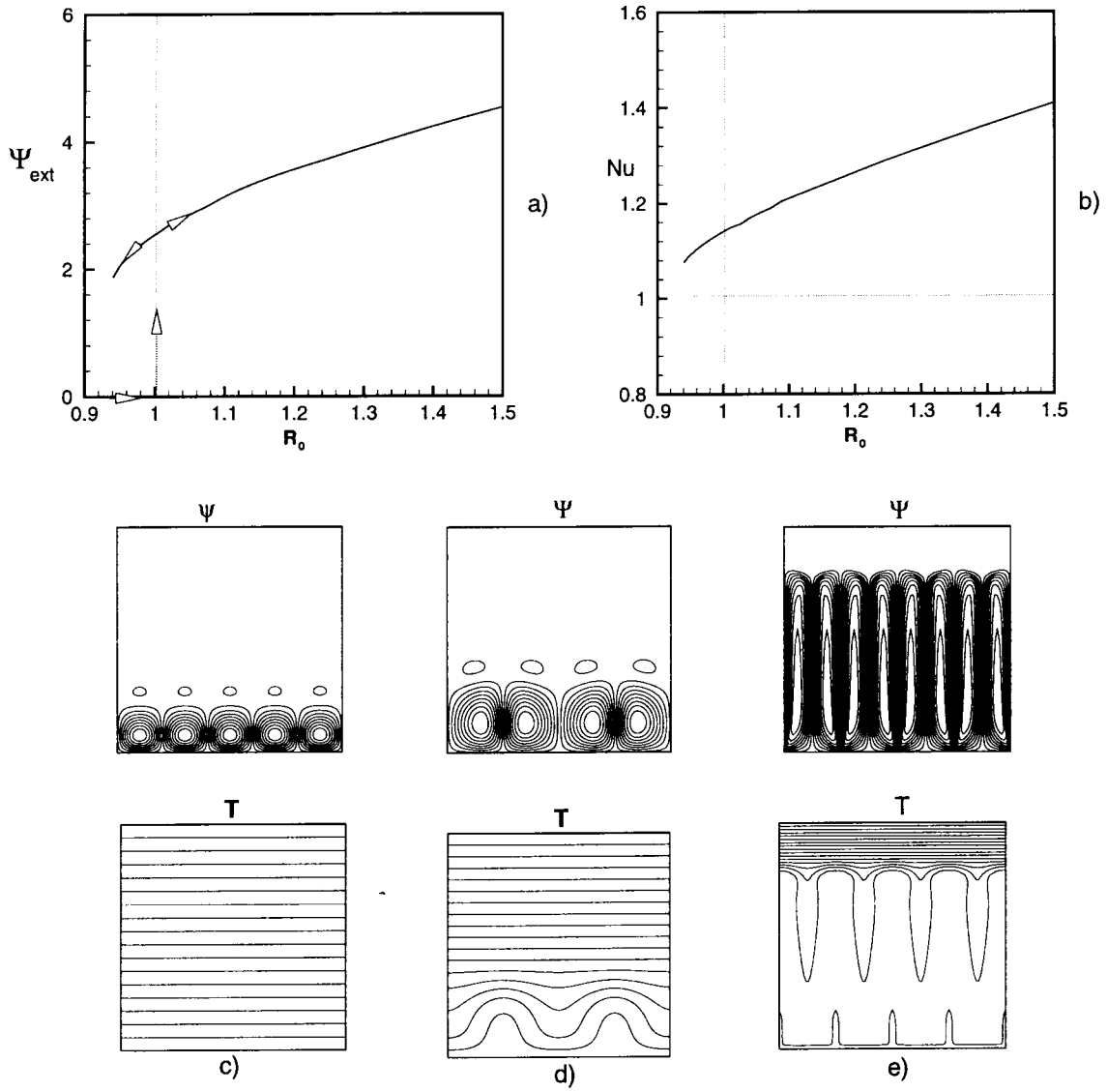

Fig. 8. Finite amplitude convection at $\gamma = 1/3$ for a pure Darcy medium: (a) Ψ_{ext} function of R_0; (b) *Nu* function of R_0; (c) incipient flow pattern and isotherms ($R_{mC} = 29.78$); (d) and (e) flow patterns and isotherms at $R_0 = 1$ and $R_0 = 12.4$, respectively.

This particularity, which is in contrast with standard Bénard convection, is attributed to the non linear source term in the momentum equation. From a mathematical point of view, it can be easily demonstrated that if $\Psi(x, y)$ and $T(x, y)$ are a solution of the present problem $\Psi(-x, -y) \neq \Psi(x, y)$ and $1-T(-x, -y) \neq T(x, y)$ since the density exhibits a quadratic variation in temperature, T. Therefore, the solution for finite amplitude convection is not symmetric (this lack of symmetry has already been noticed by Moore and Weiss [10]).

For $\gamma = 1/3$, the resulting incipient flow field corresponding to the critical Rayleigh number, ($R_{mC} = 29.78$), contains five cells. However, the finite amplitude curve shown in Fig. 8(a) and (b) stands for solutions having a four-cell flow pattern and extends below R_{mC} (subcritical bifurcation). The flow field and its corresponding temperature field, obtained at $R_0 = 1$, are shown in Fig. 8(d). Although the solution is obtained exactly at R_{mC}, the isotherms are strongly distorted, this behavior being typical of a subcritical bifurcation. The path shown by arrows in Fig. 8(a) is the one that can be followed to test the character of the subcritical bifurcation and to obtain the curve

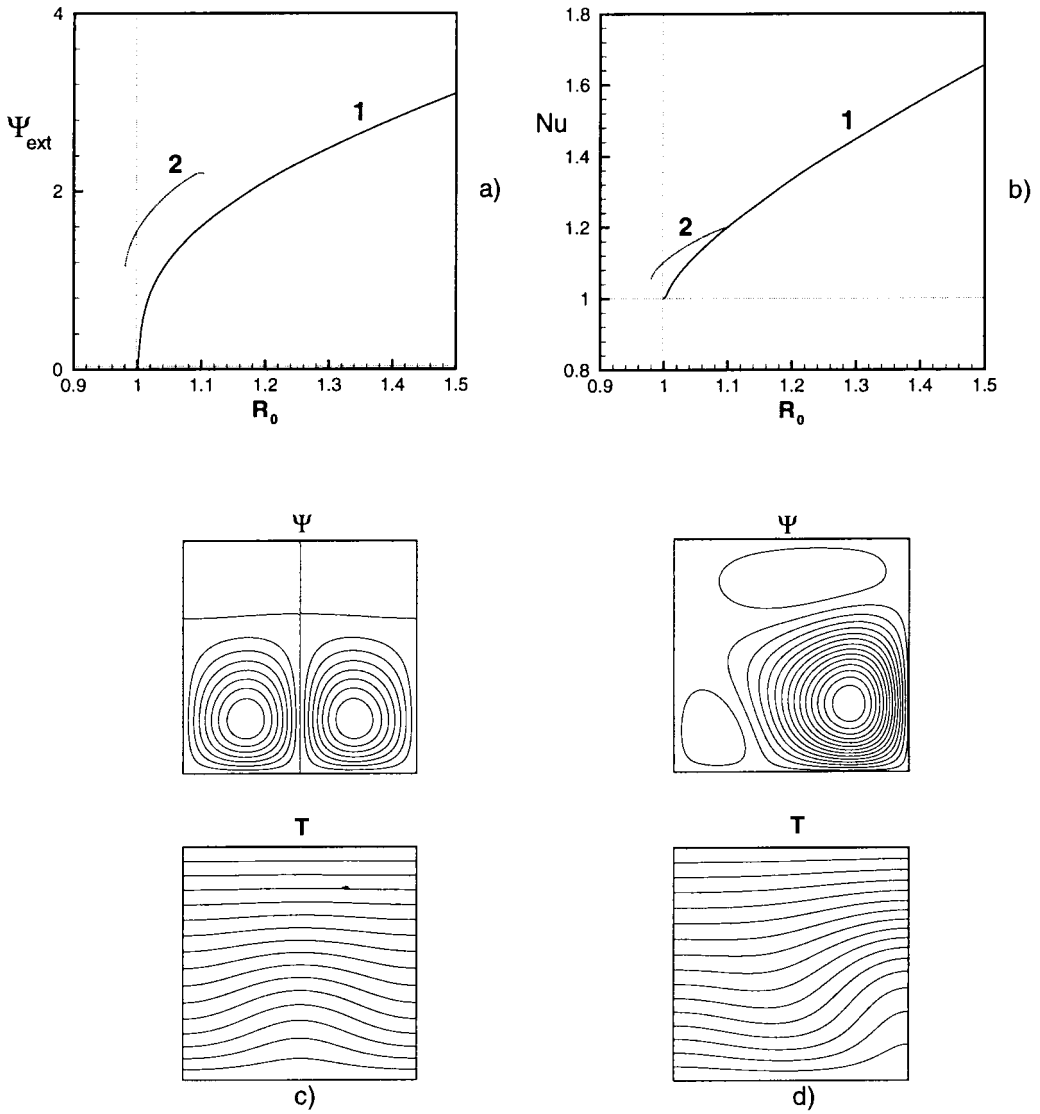

Fig. 9. Finite amplitude convection at $\gamma=1$ for a pure Darcy medium: (a) Ψ_{ext} function of R_0; (b) Nu function of R_0; (c) and (d) flow patterns and isotherms at $R_0=1.01$ corresponding, respectively, to curves labeled 1 and 2.

representing the locus of steady state solutions. One starts at $R_0 < 1$ with pure conduction ($\Psi=0$ and $T=T_R$) as initial condition to which is superposed a small perturbation. For all tests below $R_0=1$, the perturbation is resorbed with time and the pure conduction recovered. At R_0 barely larger than unity, any small perturbation will bring the system to the finite amplitude level of the curve. Using those new results as initial conditions, one can get other results at neighbouring points and repeat the procedure to obtain the whole range $0.94 \leq R_0 \leq 1.5$.

For $\gamma=1/3$, the pure conduction unstable layer has a depth corresponding to $(\gamma H'/2)$. The incipient penetration, Fig 8(c), already exceeds the depth of the unstable layer. One can notice that the actual penetration of the flow field, Fig. 8(d), at $R_0=1$ is even larger than the incipient penetration. The temperature field in Fig. 8(d) shows two distinct regions. The lower one is characterized by convection and the upper one by pure conduction with isotherms regularly spaced. A whole family of solutions may thus be defined from the actual one, by truncating or extending the pure conduction region, i.e. by changing the location of the upper boundary and setting the appropriate boundary temperature. The penetration observed in Fig. 8(d) is amplified with increasing Rayleigh number. Fig. 8(e) at

$R_0 = 12.4$ shows a penetration that reaches 80% of the total depth. At this level of convection the flow pattern contains eight convective cells. The multiplication of cells with increasing R_0 is a normal phenomenon found in standard (ρ vs T) linear convection with bottom heating. However, the penetration effect is a characteristic of convection involving a maximum density.

For $\gamma = 1$ ($R_{mC} = 31.5$), there are two solutions possible above R_{mC}, as shown by the two curves of Fig. 9(a) and (b). One curve corresponds to the standard Bénard behavior (supercritical convection) with Ψ_{ext} decreasing to zero as R_m approaches R_{mC} from the upper values. The other curve has a finite value of Ψ_{ext} extending below R_{mC} (subcritical convection) and a Nusselt number above unity. The first solution was computed up to $R_0 = 1.5$, by using the rest state as initial condition. The second curve was initiated using a unicellular finite amplitude flow as initial condition at a Rayleigh number above the critical value. Subsequent results were obtained by using previous results as initial values to extend the curve at lower and higher Rayleigh numbers. With this procedure, it was possible to obtain stable solutions for the narrow range $0.97 \leq R_0 \leq 1.1$.

Fig. 9(c) and (d) are flow and temperature fields corresponding to the first and second types of solutions, respectively, both at $R_0 = 1.01$. The flow field illustrated in Fig. 9(c) is quite similar to the corresponding incipient flow field shown in Fig. 2(b). It is very weak and has little effect on the isotherms. The other flow field, Fig. 9(d), which contains one main cell, although at $R_0 = 1.01$, produces a more important distortion of the isotherms. As a result, the heat transfer rate is greater than unity in the neighbourhood of the bifurcation point (see the dotted curve in Fig. 9(b)). To the authors' knowledge, the existence of such multiple solutions for the case of convection in cold water has not been reported yet.

6. Conclusions

A stability study has been performed for the case of a horizontal Brinkman porous layer of finite/infinite lateral extent, saturated with water in the neighbourhood of 4°C. Critical Rayleigh numbers have been obtained as functions of the Darcy number, the aspect ratio of the enclosure and the inversion parameter, this last one defining the vertical position of the maximum density with respect to the horizontal boundaries. Results have been brought to a simple form by the use of a particular definition for the Darcy number and aspect ratio, based on the thickness of the unstable layer in replacement of the total depth.

Finite amplitude computations for a Darcy medium have revealed the existence of convective motion below the threshold established by a linear stability analysis, when γ is smaller than unity. This type of behavior which corresponds to subcritical bifurcation has already been observed by Moore and Weiss [10] for the fluid case.

Acknowledgements

Financial support by Natural Sciences and Engineering Council of Canada and FCAR of Province of Quebec are acknowledged.

References

[1] C.W. Horton, F.T. Rogers, Convection currents in a porous medium, Journal of Applied Physics 16 (1945) 367–370.
[2] E.R. Lapwood, Convection of fluid in a porous medium, Proceeding of Cambridge Philosophiae Society 44 (1948) 508–521.
[3] D.A. Nield, A. Bejan, Convection in Porous Media, Springer-Verlag, New York, 1992.
[4] Z.S. Sun, C. Tien, Y.C. Yen, Onset of convection in a porous medium containing liquid with a density maximum, in: Prococeeding of the Fourth International Heat Transfer Conference, Paris, Versailles, paper NC 2.11, 1972.
[5] Y.C. Yen, Effects of density inversion on free convection heat transfer in a porous layer heated from below, International Journal of Heat Mass Transfer 17 (1974) 1349–1356.
[6] K.R. Blake, D. Poulikakos, A. Bejan, Natural convection near 4°C in a water saturated porous layer heated from below, International Journal of Heat Mass Transfer 27 (1984) 2355–2363.
[7] D. Poulikakos, Onset of convection in a horizontal porous layer saturated by cold water, International Journal of Heat Mass Transfer 28 (1985) 1899–1905.
[8] Zhang X Wave Number Selection in penetrative Convection. Ph.D. thesis, Civil Eng., Ecole Polytechnique of Montréal (1989).
[9] H.C. Brinkman, Calculation of viscous force exerted by a flow in a fluid on a dense swarm of particles, Applied Scientific Research A.1 (1947) 27–34.
[10] D.R. Moore, N.O. Weiss, Nonlinear penetrative convection, Journal of Fluid Mechanics 61 (1973) 553–581.
[11] S. Musman, Penetrative convection, Journal of Fluid Mechanics 31 (1968) 343–360.
[12] P. Vasseur, L. Robillard, The Brinkman model for boundary layer regime in a rectangular cavity with uniform heat flux from the side, International Journal of Heat and Mass Transfer 30 (1987) 717–727.
[13] J.K. Platten, J.C. Legros, Convection in Liquids, Springer-Verlag, New York, 1984.
[14] S. Chandrasekhar, Hydrodynamic and Hydromagnetic Stability, Oxford University Press, London, 1961.